Covalent assembly of nanoparticles as a peptidase-degradable platform for molecular MRI

Francisco Perez-Balderas[1,2], Sander I. van Kasteren[2,6], Alaa A.A. Aljabali[2,3,8], Kim Wals,[2,4] Sébastien Serres[1,9], Andrew Jefferson[3], Manuel Sarmiento Soto[1], Alexandre A. Khrapitchev[1], James R. Larkin[1], Claire Bristow[1], Seung Seo Lee,[2,7] Guillaume Bort,[2] Filippo De Simone,[2] Sandra J. Campbell[1], Robin P. Choudhury[3], Daniel C. Anthony[4,5*], Nicola R. Sibson[1,5*], Benjamin G. Davis[2,5*]

[1]Cancer Research UK & Medical Research Council Oxford Institute for Radiation Oncology, Department of Oncology, University of Oxford, Oxford, OX3 7DQ,UK

[2]Department of Chemistry, University of Oxford, Chemistry Research Laboratory, Oxford, OX1 3TA,UK.

[3]Department of Cardiovascular Medicine and Oxford Acute Vascular Imaging Centre, University of Oxford, John Radcliffe Hospital, Oxford, OX3 9DU, UK.

[4]Department of Pharmacology, University of Oxford, Oxford, OX1 3QT, UK.

[5]These authors contributed equally to this work.

[6]Current address: Gorlaeus Laboratory, Leiden Institute of Chemistry, Leiden University, Einsteinweg 55, The Netherlands.

[7]Current address: School of Chemistry, Faculty of Natural and Environmental Sciences, University of Southampton, Highfield, Southampton, SO17 1BJ, UK.

[8]Current address: Pharmacy Department, Yarmouk University, Irbid, Jordan.

[9]Current address: School of Life Sciences, University of Nottingham, NG7 2UH, UK.

*Correspondence should be addressed to DCA (daniel.anthony@pharm.ox.ac.uk), BGD (ben.davis@chem.ox.ac.uk) or NRS (nicola.sibson@oncology.ox.ac.uk)

28

29

Abstract

Ligand-conjugated microparticles of iron oxide (MPIO) have the potential to provide high sensitivity contrast for molecular magnetic resonance imaging (MRI). However, the accumulation and persistence of non-biodegradable micron-sized particles in liver and spleen precludes their clinical use and limits the translational potential of MPIO-based contrast agents. Here we show that ligand-targeted MPIO derived from multiple iron oxide nanoparticles covalently may be coupled through peptide linkers that are designed to be cleaved by intracellular macrophage proteases. The synthesised particles possess potential characteristics for targeted MRI contrast agents, including high relaxivity, unappreciable sedimentation, clearance from circulation and no overt toxicity. Importantly, we demonstrate that these particles are rapidly degraded both *in vitro* and *in vivo*, and that the targeted probes can be used for detection of inflammation *in vivo* using MRI. This approach provides a platform for molecular MRI contrast agents that is potentially more suitable for translation to humans.

INTRODUCTION

The high magnetization and low toxicity of superparamagnetic iron oxide particles has led to their widespread use in biomedical and biological applications[1-3] including MRI[4,5], cancer therapy[6], cell labelling[7], biomolecule sensing[8,9] and multimodal imaging[10]. These particles can be synthesized across a range of diameters, of which the ultrasmall superparamagnetic particles of iron oxide[5] (USPIO; 20-50 nm in diameter) have been clinically used the most. The long circulation half-life of USPIO precludes rapid molecular imaging of target-specific binding owing to high background levels[11]. In contrast, microparticles of iron oxide (MPIO) have a short half-life (< 5 min[12]) in the circulation and greater contrast-to-noise per particle than USPIO owing to their higher iron content (0.26 pg iron/particle vs 1.1×10^{-6} pg iron/particle). Moreover, the increased surface area of MPIO (*ca*. 2 - 12 μm^2) compared with USPIO (*ca*. 0.005 - 0.03 μm^2) enables greater ligand valency, which can substantially increase binding affinities through multivalent effects[13,14]. In this context, the strong correlation between target quantification in tissue and contrast volume on non-invasive MRI points strongly towards the advantages of MPIOs.[15] The potential of MPIO for imaging diagnostically useful endovascular cellular events, such as inflammation and activated platelet adhesion, has already been highlighted in a range of animal models of important human disease, including multiple sclerosis[16,17], thrombosis[18], atherosclerosis[19], renal[15] and cerebral ischaemia[16,20], cerebral malaria[21] and brain metastases.[22] If such MPIO could be synthesised in a biodegradable form, they have the potential to provide superior capabilities for molecular imaging of disease in humans.

Although regulatory approval must of course be considered on a case-by-case basis, we consider that translation to clinical use requires a number of essential attributes: biocompatibility, high iron content, controlled biodegradability, functionalisable surface with multivalent capacity, appropriate shape to promote multivalent binding to the planar

endothelial surface, short blood half-life, minimal non-specific accumulation and low tendency to agglomerate. Here, we describe a microparticle system designed through covalent assembly of multiple iron oxide nanoparticles, which combines the advantages of the micron-size iron particle range with biodegradability via the endogenous clearance[23-25] and degradation systems of the body (**Fig. 1**, **Supplementary Fig. 1**). These microparticles are therefore deserving of further research for their potentially enhanced utility as *in vivo* imaging agents and potential clinical application as iron-based molecular MRI contrast agents.

RESULTS

mMPIO Construction via Iron Oxide Nanoparticle Conjugation

Biodegradable multimeric microparticles of iron oxide (mMPIO) were covalently assembled from multiple colloidal iron oxide nanoparticles (NPs) of diameter 65 nm bearing an amine-funtionalized dextran coat (**Fig. 2**). These common precursor particles (**Supplementary Fig. 2,3** and **Supplementary Tables 1-2**) were then elaborated into two complementary nanoparticle subtypes that could be readily coupled together. In the first subtype carboxylate groups were created from amino groups using succinic anhydride to form carboxy-NPs[26] (**Supplementary Fig 3**). In the second, peptide sequences were added to create peptido-NPs (**Supplementary Fig 3 and Supplementary Table 3**). These peptide sequences were carefully designed to provide, not only, a suitable linker between monomer particles, but also a linker that would be sensitive to specific intracellular degradative enzymes. Such proteases have previously been shown to display strong potential in, for example, targeted toxin release systems[27,28] and differential regulation in some disease states.[29] The cathepsin proteins are the

primary degradative enzymes in macrophages, which are the main site of sequestration of iron oxide particles in the liver and spleen on clearance from the circulation[30-32]. The proteolytic activity of lysosomal cathepsin B (EC 3.4.22.1) and L (EC 3.4.22.15) was tested against possible consensus peptide sequences[33-35]. The most efficiently cleaved (**Supplementary Figs. 4-8**) yet plasma stable (**Supplementary Figs. 9-10**) peptide was chosen and incorporated. Stability of this peptide under serum conditions was also tested (**Supplementary Figs. 11-13**); assays revealed degradation following clotting of blood but stability upon treatment with EDTA (**Supplementary Fig. 13**), suggesting susceptibility to metal-dependent proteases induced in the clotting cascade (e.g. Factor IXa and XIa). To stringently test the specificity of these chosen sequences we created four homologues of the Cathepsin L specific peptide Fmoc-Ahx-Ahx-FVRGAGE (**Supplementary Figure 4**). In these homologues, key residues were varied or scrambled, and D-amino acids were used (including a 'mirror-image' peptide). When examined in detail, through the kinetics of cleavage combined with MS analysis (see **Supplementary Figs 14-17 and Supplementary Table 5**), these revealed much lower cleavage activity towards the scrambled and particularly the D-amino acid peptide, as expected.

Using the carboxy-NP and peptido-NP monomers, larger multimeric microparticles of iron oxide (mMPIO) were synthesized. This synthesis was performed using robust amide-forming chemistry in MES buffer pH 6.0 via N-hydroxysulfosuccinimide (sulfoNHS) ester[36]. The resulting panel of mMPIO was characterized and optimized for key parameters including size, yield and reactivity (**Fig. 3a and Supplementary Table 4**). Combined Electron Microscopy (EM), Transmission Electron Microscopy (TEM), Atomic Force Microscopy (AFM), zeta potential and Dynamic Light Scattering (DLS) measurements confirmed construction and the anticipated morphology and characteristics of our designed larger, multimeric particles (**Fig 3b and Supplementary Fig 18 and Supplementary Table 4**).

Composition and dextran content were further confirmed by chemical and elemental analysis. Importantly, by varying the reaction ratio of the two monomer types it was possible to change both the particle size and the nature of the surface reactive functional groups of the resulting mMPIO (**Fig 3a** and **Supplementary Table 4**), which in turn would ensure that a broad range of targeting ligands could be conjugated. This approach, therefore, allowed us to readily create mMPIO bearing either an excess of amine (mMPIO-NH_2) or those bearing an excess of carboxylic acid (mMPIO-COOH).

mMPIOs Show Low Sedimentation and High MRI Relaxivities

We have previously shown that microparticles of 0.5 - 1 μm diameter combine favourable characteristics of high contrast effect and rapid blood phase clearance rate that are well suited to *in vivo* targeting studies[16], by delivering efficient particle binding to the site of interest and low background signal at the time of MRI. At the same time, the MPIO are still much smaller than erythrocytes and not prone to microvascular plugging. mMPIOs within this size range were efficiently and reliably constructed through modulation of the starting ratios of the two monomers (**Fig. 3a**). These mMPIO exhibited physicochemical advantages over equivalent monomeric iron-dextran MPIO (~ 0.7 μm diameter; see **Supplementary Method 10** for synthesis). In particular the mMPIO showed very little tendency to precipitate, with sedimentation rates markedly lower than correspondingly sized monomeric particles and commercially available polystyrene coated particles (<1, 51 and 86 % of sedimentation at 24 h, respectively; **Supplementary Figs. 19-20**); such effects potentially increase the translational potential of the mMPIOs and may be due to crosslinking or surface charge changes (although they are consistent with many different surface potential levels, **Supplementary Fig. 3**). Moreover, the mMPIO displayed storage stability at 4 ºC for more than six months (**Fig. 3c**); They also exhibited significantly higher T_2 relaxivities (194.5 ± 4.5

145 $mM^{-1}s^{-1}$ at 4.7 T and 196.5 ± 4.9 $mM^{-1}s^{-1}$ at 7 T; **Fig. 3d, Supplementary Fig 21 and**
146 **Supplementary Table 7**) than commercially-available polystyrene coated particles (58.5 ±
147 2.2 and 59.5 ± 1.2 $mM^{-1}s^{-1}$ at 4.7 T and 7 T, respectively, **Supplementary Table 7**) that have
148 previously[16] demonstrated good contrast in vivo, potentially due to previously noted magnetic
149 relaxation switch phenomena.[9]
150
151 *mMPIO are Biodegraded In Vitro and In Cellulo*
152 Next, the biodegradability of the mMPIOs was evaluated *in vitro*. Consistent with their
153 molecular design, incubation of mMPIOs with both cathepsins B and L efficiently degraded
154 the peptide linker yielding the monomeric NPs from which they were built (**Fig. 4a**). Having
155 demonstrated the biodegradable nature of the linker with respect to the appropriate enzymes,
156 cellular uptake and intracellular degradation of the mMPIO was evaluated. Both amino-
157 terminated mMPIO (mMPIO-NH_2) and carboxylic acid-terminated mMPIO (mMPIO-
158 COOH) (entry 3 and 7 from **Fig. 3a**, respectively) were labelled with the fluorophore
159 AlexaFluor 488 cadaverine. These fluorescently-labelled mMPIO were incubated with
160 cultured macrophages. Confocal time course experiments showed a consistent and clear
161 reduction in the number of intracellular mMPIO over 12 hours (**Fig. 4b**, **Supplementary**
162 **Figs. 22,23** and **Supplementary Movie 1**). Further experiments (**Supplementary Figs.**
163 **24,25**) showed that punctuate fluorescence in the intracellular compartment faded over time.
164 After 72 h, the fluorescence was homogeneously distributed and no large particles were
165 detectable, suggesting complete degradation. By comparison, the equivalent large (733nm)
166 amino-terminated monomeric MPIO remained intact after 48 h, with only slight degradation
167 after 72 h (**Supplementary Fig. 26**), suggesting a considerably slower rate of degradation
168 compared to the mMPIO. Cellular uptake of the mMPIOs was confirmed and subcellular
169 distribution of the degradation products was also analyzed in macrophage cell-line (RAW

264.7) using Transmission Electron Microscopy (TEM, see **Supplementary Fig. 27**) over 72 h. Upon internalization into the distinctive cell morphology of the cells, mMPIOs were clearly surrounded by visible membrane structures suggesting anticipated formation of endolysosomal compartments within which the structure of the mMPIO degraded. This confirmed the uptake into phagosomes of high intensity material containing iron and then its loss over time. In contrast, commercially-available monomeric MPIO beads remained intact (with high iron content) throughout. We also constructed mMPIOs linked by peptides containing D-amino acids in the same sequence used for the degradable mMPIOs; consistent with the resistance shown by D-amino acid-containing peptides to cathepsins, these "D"-mMPIOs were not degraded (**Supplementary Figures 28-32**). These experiments further supported both the efficacy and the molecular mechanistic basis of the designed degradable "L"-mMPIO system.

mMPIOs are not Non-Specifially Retained and Clear Rapidly

Having confirmed *in vitro* degradation of the mMPIO, the *in vivo* biodistribution and clearance of the mMPIO were evaluated histologically (**Figs. 4c,d** and **Supplementary Figs**. **33,34**). Both mMPIO-NH_2 and the equivalent size amino-terminated monomeric MPIO were injected intravenously into naïve mice. Primary uptake of both the mMPIO and monomeric MPIO was evident in the liver 1h after injection, and in both cases the particles were almost entirely cleared from this site by 7 days. Low-level mMPIO retention was also observed in the intestine and lung at 1h, although the level of particle staining was low compared to that observed in the liver (0.001 and 0.044, respectively, vs. 0.208% area stained) and, again, was negligible by 7 days. Similar low levels of monomeric MPIO retention were found in the intestine. In striking contrast, substantial monomeric MPIO retention was evident in the lungs, which was lower but still evident 14 days post-injection (*ca*. 1% tissue area). The

lung is known to play an important role in removing blood-borne foreign bodies via adherent phagocytes and endothelial cells, and particles cleared this way are passed through the endothelium to accumulate in macrophages in the alveolar interstitium.[37] Thus, it might be expected that MPIO would also be cleared from the circulation by this pathway. Unlike the MPIO, however, the mMPIO were not cleared to any appreciable extent via the lungs (*cf.* 1 hour data, **Fig. 4c,d** and **Supplementary Fig. 34**), reflecting their different physicochemical properties. Very low and constant levels of iron staining were evident in the white pulp of the spleen in both mMPIO and MPIO injected animals (0.1 – 0.2 % tissue area), whilst the very high intrinsic iron levels in the red pulp of the spleen precluded quantitation of the small increases arising from mMPIO/MPIO accumulation. No appreciable retention of the mMPIO or monomeric MPIO was found in heart, brain or kidney (< 0.0005% of tissue area, **Supplementary Fig. 33**). Importantly for our goal of creating a flexible particle system, chemical surface functionality did not alter *in vivo* distribution; no appreciable differences were seen in animals injected with mMPIO-COOH compared to those injected with mMPIO-NH_2.

In order to assess whether labelling of the mMPIO with targeting antibodies altered the clearance profile and to obtain formal toxicological data, pre-clincial studies were conducted (Sequani Ltd., see **Supplementary Method 16**) in which mice were injected with mMPIO conjugated to a humanised anti-human-VCAM-1 antibody (αhuVCAM) with cross-reactivity to mouse (αhuVCAM -mMPIO). All values for clinical observations (body weight, organ weights, macroscopic histology) were within normal ranges, and no blood chemistry (**Supplementary Tables 9-10**), haematology (**Supplementary Tables 11-12**) or histology findings (**Supplementary Fig. 35**) were of toxicological significance. In accord with our findings above, a very low level of diffuse iron staining was found in the liver 2 days after administration of αhuVCAM-mMPIO in 5/6 mice, which was no longer evident by 14 days

post-αhuVCAM-mMPIO injection (**Supplementary Fig. 35**). In-house quantitative analysis confirmed the absence of particulate iron deposits (i.e. undegraded mMPIO) at both 2 and 14 days post-αhuVCAM-mMPIO injection, indicating degradation within the first 48h period. No αhuVCAM-mMPIO retention was evident in any other tissue, or in control animals, at either time point. Thus, the biodistribution profile of the mMPIO remained the same when conjugated to a targeting antibody. Since VCAM-1 is not highly expressed on vascular endothelium under normal conditions, accumulation in tissue beds expressing VCAM-1 other than the brain has not been examined, as this would require different disease models. No evidence of infarction or inflammation was found in any of the organs studied in any of the above studies, up to 14 days post-mMPIO injection.

Antibody-targeted mMPIOs Allow Molecular Imaging

Having established biodistribution profiles, the utility of this platform to create targeted mMPIOs as tools for molecular imaging was tested. The diversity of functional groups in the mMPIOs, which is a consequence of their multimeric assembly, also allowed ready orthogonal labelling such that different ligands could be incorporated via different functional groups (**Supplementary Fig. 36**). In this way mMPIOs were created that contained both multiple fluorescent labels in the inner core of the particle and high levels of surface targeting moieties. Particles were synthesised bearing either an anti-VCAM-1 antibody (αVCAM) or a corresponding IgG control antibody (αVCAM-AF488-mMPIO and IgG-AF488-mMPIO, respectively). Both targeted particles exhibited similarly high surface antibody density (**Supplementary Fig. 37**). As expected αVCAM-AF488-mMPIO, but not IgG-AF488-mMPIO, showed high binding capacity towards activated endothelial cells *in vitro* (**Supplementary Fig. 38**).

Finally, the potential of the αVCAM-AF488-mMPIO for *in vivo* molecular MRI was evaluated in a mouse model of cerebral inflammation. Mice were injected intracerebrally with IL-1β in the left striatum, to induce endothelial activation and VCAM-1 expression.[16] In animals subsequently injected intravenously with αVCAM-AF488-mMPIO a marked contrast effect was evident on the T2*-weighted images, manifest as focal hypointensities in the IL-1β-injected hemisphere (**Fig. 5a,c, Supplementary Fig 39a and Supplementary Movie 2**). Notably, the contrast effect was unilateral with no non-specific mMPIO-induced hypointensities in the non-injected hemisphere. Negligible contrast effects arising from mMPIO retention were present in any of the controls: (i) naïve mouse injected intravenously with αVCAM-AF488-mMPIO; (ii) mouse injected intracerebrally with saline and intravenously with αVCAM-AF488-mMPIO; and (iii) mouse injected intracerebrally with IL-1β and intravenously with the non-targeted IgG-AF488-mMPIO (**Fig. 5b,d, Supplementary Fig. 39b** and **Supplementary Movie 3**). Quantitative analysis of the volumes of hypointensity induced by αVCAM-AF488-mMPIO binding yielded substantially greater volumes in the IL-1β-injected animals than in any of the control animals (**Fig. 5e**). Subsequent T_1-weighted images acquired after intravenous administration of the passive contrast agent gadolinium-DTPA revealed no areas of contrast enhancement in any animal, verifying that the blood-brain-barrier (BBB) was intact. Taken together, these data indicate specific binding of αVCAM-AF488-mMPIO to acutely activated endothelium in the absence of BBB breakdown.

Following the *in vivo* MRI experiments, co-localisation of VCAM-1 expression and αVCAM-AF488-mMPIO binding was verified both immunohistochemically and by immunofluorescence (**Fig. 5f-i**). Immunohistochemical analysis demonstrated upregulation of VCAM-1 in the IL-1β-injected, but not the contralateral, hemisphere. Subsequent Prussian

Blue detection of iron revealed the presence of bound αVCAM-AF488-mMPIO in VCAM-1-positive vessels (**Fig. 5f**). Both epifluorescence and confocal microscopy of the brain sections further confirmed successful co-localisation of the αVCAM-AF488-mMPIO with both VCAM-1 and laminin, indicating association of the targeted mMPIO with VCAM-1-positive vessels (**Fig. 5g-i**).

DISCUSSION

We have demonstrated here some potential advantages conferred by the use of covalent linkages for the synthesis of mMPIO that include control of size and enhanced stability. These are both pre-requisites for clinical use of the agent that are not provided by, for example, current methodologies based on non-covalent linkages[8,9].

We have demonstrated here these mMPIOs as intra-vascular agents. In the system we propose here, molecular targeting is determined by a surface-displayed binding agent on the particle and an appropriate 'biomarker' binding partner on the cell-surface. We should add the clear caveat that we have only tested a single targeting antibody type (anti-VCAM); other important target sites also exist (e.g. interstitial space or poorly vascularized tumour cells) for imaging on which they might be tested also in the future. However, at such sites targeted agents may lose their molecular selectivity since they can also accumulate passively.

The choice of a cathepsin-cleavable peptide as the linker ensured rapid degradation of the mMPIO once sequestered by macrophages, primarily within the liver following clearance from circulation[30,31], while particles that associate with their target remain unaltered and functional. Rapid sedimentation, slow degradation and mechanical retention in organs,[23,24] such as the lung, make the corresponding monomeric MPIO particles unsuitable for use in man. In contrast, the mMPIO appear to possess properties that are useful for clinical application of molecular imaging, such as high relaxivity, unappreciable sedimentation rate,

rapid degradation, no overt toxicity and fast clearance from circulation. Due to these mechanistic differences, unlike toxic particles where dose would be rapidly limiting, excesses of mMPIO can advantageously be used. In this way, percentage binding can be even tuned accordingly, since any excess that does not bind is non-toxic, cleared rapidly and degraded. This therefore provides both a vital mechanistic and potential translational advantage. Thus, whilst key additional translational hurdles will need to be considered in even greater detail for future development and regulatory approval (i.e. stability, reproducibility, dispersity), we believe that these proof-of-principle experiments with mMPIO might provide a promising platform for the clinical use of molecular MRI contrast agents.

ACKNOWLEDGMENTS

This work was funded by a Cancer Research UK Programme Grant – C5255/A12678 (NRS), MRC DPFS Grant G0902181 (NRS, DCA, RPC, BGD) a Research Grant from Glycoform Limited (BGD), an Isis Innovation Fund Award (DCA, BGD, SvK), an EPSRC Platform Grant EP/E000614/1 (BGD), a Royal Society Wolfson Research Merit Award (BGD) and a Senior Fellowship from The Wellcome Trust (RPC). The authors would like to thank Dr Jo Peach for helpful discussions in the early stages of concept development, Mick Woodcock for flow cytometry experiments, Dr. Michael Stratford for his help with the HPLC-MS measurements and Dr. Lisa Folkes for help with HPLC analyses.

AUTHOR CONTRIBUTIONS

DCA, RPC, BGD, SIvK and NRS jointly conceived the need for a biodegradable, low-density MPIO with the clearance characteristics and size range of the particles described herein. DCA, BGD, SIvK devised a molecular strategy for synthesis of such a particle. BGD, SIvK, AA, KW, GB and FP-B, were responsible for the particle construction including physicochemical analysis, characterization, degradation kinetics and enzymatic processing. FP-B, SSL, GB and FdeS performed peptide specificity experiments. FP-B and AA optimised the particle synthesis and characterisation, and synthesized compounds for the biological studies. AK, FP-B and NRS performed the relaxivity experiments. DCA, RPC, BGD and NRS designed the biological studies. AJ, FP-B and KW performed the cellular microscopy experiments. SJC and NRS designed the formal toxicology study, which was conducted by Sequani Ltd. DCA, NRS and MSS performed the *in vivo* biodistribution experiments. DCA,

JL, MSS, SS and NRS performed the in vivo MRI experiments. CB, JL and MSS conducted the histological measurements on resulting tissue samples. DCA, BGD, AJ, JL, FP-B, SS, MSS and NRS analysed the biological data. DCA, SJC, RPC, BGD, SIvK, FP-B and NRS prepared the manuscript. All authors read and edited the manuscript.

COMPETING FINANCIAL INTERESTS

DCA, BGD, NRS declare that a patent (WO2008035069) associated with this work has been filed. The other authors declare no competing financial interests.

DATA AVAILABILITY

All relevant data are available from the authors. Relevant raw data files for particle sizing, MRI, microscope images, HPLC chromatograms have also been placed on the Oxford University ORA-data system, doi: 10.5287/bodleian:qaY9QE2kN. All data are also available from the authors.

METHODS

General Considerations

All animal experiments were authorised by the UK Home Office. Chemical abbreviations and details of the equipment employed are given in **Supplementary Method 1**.

Synthesis of dextran covered nanoparticles

5 mmol of $FeCl_3 \cdot 6H_2O$ and 9, 10 or 12 g of dextran average mol. wt. 9000-11000 (SigmaAldrich, cat. Nr. D9260, lot Nr. 1331472 or 1382459) or 7.3 g of Dextran 10 Pharmaceutical Quality (Pharmacosmos, batch Nr. HX4271) were dissolved in 20 mL of water and deoxygenated thoroughly by repeated cycles of vacuum assisted by sonication and argon flushing. After the first deoxygenation cycle, 3 mmol of $FeCl_2 \cdot 4H_2O$ in 5 mL of water was added and the solution was deoxygenated by the above procedure (4 times). While being stirred with an overhead stirrer at 600 rpm, NH_4OH (4 mL, 25%) was added at a rate of 168 mL/h. The reaction was heated to 80 ºC and then stirred at this temperature for 1 h. The solution was cooled and placed in a SpectraPor membrane (MWCO 100000) leaving some space for volume increase. The solution was dialyzed against 5 L of water for 21 h with water changes at times 1, 2 and 4 h. Iron content was measured spectrophotometrically at 410 nm after acid dissolution (6M HCl (aq)) and oxidation (3% hydrogen peroxide solution) for 1h.[38] and adjusted to a final concentration of 10 mg Fe/mL using a Vivaspin centrifugal unit (MWCO 30.000). An aliquot (10 μL) was diluted with 700 μL of PBS and particle size was determined by DLS. A sample (5 mg of iron) was freeze dried and elemental analysis was determined (**Supplementary Method 2** and **Supplementary Table 1**).

Synthesis of amino-terminated nanoparticles

20 mL of dextran covered nanoparticles (10 mg/mL) were placed into a 250 mL round flask equipped with a 30x16 mm oval stirrer bar. While the solution was stirred at 500 rpm, 36.7 mL of NaOH 5 M was added at a rate of 168 mL/h. After that, 13.3 mL of epichlorohydrin (20 mL in case of Phamacosmos HX4271 dextran, results "k-l" Supplementary Table 1) was added at a rate of 94 mL/h. The mixture was stirred at 1000 rpm for 7 h and then 20 mL of NH_4OH (25%) was added at a rate of 168 mL/h. The mixture was stirred at 1000 rpm for 14 h and then was placed in a SpectraPor 2 or 100 kDa cut-off membrane leaving some space for volume increase. The solution was then dialysed against 5 L of water for 21h with water changes at times 1, 2 and 4 h. Fater that the solution concentrated on a Vivaspin 15 unit (MCWO 30.000) to 15 mg Fe/mL. A sample (5 mg of iron) was freeze dried and elemental analysis was determined (**Supplementary Method 2** and **Supplementary Table 2**).

Synthesis of carboxylic acid terminated nanoparticles

Succinic anhydride in DMSO (4 mL, 15 mg/mL) was added to a solution of amino-NPs (8 mL, 10 mg Fe/mL) in sodium bicarbonate buffer 100 mM pH 8.3. Note: The reaction is exothermic and a nitrogen filled balloon with a syringe was placed on the tube. The mixture was shaken for 3 h, then 4 mL of succinic anhydride in DMSO (15 mg/mL) was added and the mixture shaken for a further 3 h. The sample was dialyzed in a 10.000 Da dialysis membrane against 5 L of water for 21 h with water changes at times 1, 2 and 4 h and was concentrated in a Vivaspin 20 unit (MCWO 30.000) to 15 mg Fe/mL.

Peptide synthesis

SPPS peptide synthesis was performed under standard Fmoc-conditions using HBTU/HOBt as activator and DIPEA as base-catalyst. Deprotection and couplings were performed under microwave irradiation employing a single coupling protocol except for the first residue,

which was introduced by double coupling. Peptide cleavage was performed using TFA/TIS/H_2O 95:2.5:2.5 (10 mL/g resin). The solvent was partially evaporated and the peptide was precipitated by addition of a cold mixture of diethylether/hexane 1:1, centrifuged and washed again with the same mixture. The peptide was homogenized, dried under high vacuum for 3 h, re-dissolved in water/acetonitrile/DMSO/TFA 70:15:5:0.1 and purified by preparative RP chromatography. This product was dissolved in 2% DMSO in water and analysed by HPLC. For structure of peptides see **Supplementary Figure 4**. Peptides were characterized by HPLC, high resolution mass spectrometry and tandem mass spectrometry (MS/MS) (**Supplementary Figs. 40-47** and **Supplementary Tables 13-17**). The proteolytic activity of the cathepsins on the peptides was analyzed by HPLC (**Supplementary Methods 6-8**).

Synthesis of peptide covered nanoparticles (peptido-NPs)

A solution of EDC in water (0.84 mL, 38 mg/mL) was added to a solution of peptide 3 (200 mg) and NHS (24 mg) in DMSO (3.7 mL). This solution was incubated for 5 minutes at rt and then added to a solution of 20 mg of amino-NPs in 3.3 mL of MES buffer 0.1 M pH 6.0. The solution was shaken for 3 h at rt, and then split into two 50 mL centrifuge tubes. Particles were precipitated by addition of 45 mL of acetonitrile, centrifuged for 20 min at 3250 xg and the supernatant was carefully discarded taking care not to disturb the precipitate. The precipitate was re-suspended in 5 mL of DMSO, an aliquot (100 μL) was taken and Fmoc analysis was performed (**Supplementary Method 3**). The rest of the sample was precipitated again by addition of 45 mL of acetonitrile and centrifuged as before. Samples were re-suspended in 5 mL of DMSO and 5 mL of 40 % piperidine in DMF was added. The samples were shaken for 30 minutes after which the particles were precipitated by addition of 45 mL of 1,4-dioxane. Samples were re-suspended in 5 mL of DMSO and the deprotection step was

repeated. Precipitate was re-suspended in water, dialyzed in a 10.000 MWCO dialysis membrane against 5 L of water for 21 h with water changes at times 1, 2 and 4 h and was concentrated in a Vivaspin 6 unit (MCWO 30.000) to 15 mg Fe/mL (**Supplementary Table 3**). An essentially similar method was used for the synthesis of D-peptido-NPs containing D-amino acids in the peptide.

Synthesis of amino-terminated mMPIOs (mMPIO-NH_2)

A solution of carboxy-NPs (25.5 μL, 11.2 mg Fe/mL, 0.285 mg Fe) in MES buffer 0.1M pH 6.0 was activated by sequential addition of sulfoNHS (2 μL, 1.5 eq. respect to the N content of its amino-NPs precursor; see **Supplementary Table 2**) and of EDC (1 μL, 1.2 eq. respect to the N content of its amino-NPs precursor; see **Supplementary Table 2**) in MES buffer 0.1 M pH 6.0. The resulting solution was shaken and incubated at rt for 5 minutes and added to a solution of peptido-NPs (171 μL, 10 mg/mL, 1.71 mg Fe) in MES buffer 0.1 M pH 6.0. The reaction was shaken at 55 ºC for 24 h at 1400 rpm. Once the reaction had finished the sample was diluted and purified by dialysis and either by magnetic pelleting (**Supplementary Method 4**) or by sucrose gradient (**Supplementary Method 5**). An aliquot (2 μL) was redispersed in 700 μL of PBS and size was measured by DLS (**Supplementary Table 4**). An essentially similar method was used for the synthesis of the D-amino-acid-mMPIOs from D-peptido-NPs.

Synthesis of carboxy-terminated mMPIOs (mMPIO-COOH)

A solution of carboxy-NPs (122 μL, 15.3 mg Fe/mL, 1.71 mg Fe) in MES buffer 0.1 M pH 6.0 was activated by sequential addition of sulfoNHS (15 μL, 1.5 eq. respect to the N content of its amino-NPs precursor; see **Supplementary Table 2**) and of EDC (10 μL, 1.2 eq. respect to the N content of its amino-NPs precursor; **Supplementary Table 2**) in MES buffer 0.1M

pH 6.0. The resulting solution was shaken and incubated at rt for 5 minutes and added to a solution of peptido-NPs (22.8 μL, 12.5 mg/mL, 0.285 mg Fe) in MES buffer 0.1 M pH 6.0. The reaction was shaken at 55 ºC for 24 h at 1400 rpm. Once the reaction had finished the sample was diluted and purified by dialysis and either by magnetic pelleting (**Supplementary Method 4**) or by sucrose gradient (**Supplementary Method 5**). An aliquot (2 μL) was redispersed in 700 μL of PBS and particle size measured (**Supplementary Table 4**).

Sedimentation of particles

A solution of mMPIO or 733 nm MPIO (for synthesis see **Supplementary Method 10**) (0.11 mg Fe/mL) was placed, after vortexing and sonication, in a quartz cuvette equipped with PTFE stopper. Absorption was measured at λ = 500 nm for 24 h at 5 minutes time intervals.

Relaxivity of compounds

Phantoms were prepared by addition of 0.75 mL of an agarose solution (12 %) to 0.75 mL of serial dilutions of the contrast agent in a Nalgene Cryoware vial. Samples were centrifuged at 1000 g for 5 minutes to eliminate air bubbles. MRI experiments were performed on Magnex 4.7T or 7.0T superconductive magnet driven by Varian DirectDrive™ spectrometer (Magnex Scientific and Varian Inc.; subsidiaries of Agilent Technologies, Santa Clara, CA, USA). A spin-echo sequence was used to acquire T_2 and T_1 maps. Single slice images were acquired with a matrix size of 128 x 128 pixels in all cases, corresponding to voxel dimensions of 0.4 x 0.4 x 5.0 mm. T_2 maps were generated from a series of spin echo images (repetition time (TR) = 3.0s) in which the echo time (TE) was logarithmically distributed in 10 steps from 9.7 ms to 100 ms. The total experimental time was *ca* 1 hour. T_1 maps were generated from a series of inversion recovery spin echo images (TR = 10.0 s; TE = 9.7 ms) in which the inversion recovery time was logarithmically distributed in 10 steps from 10 ms to 6.0 s. The

total experimental time was *ca* 3.5 hours. The relaxation maps were calculated using a standard mono-exponential fit employing a least squares procedure.

In vitro degradation of mMPIO by cathepsin L

Cathepsin L (0.88 μg) in 98 μL of citrate buffer 0.1 M pH 5.0 containing 1 mM EDTA was activated by addition of DTT (2 μL, 100 mM in water). After 15 minutes at room temperature this pre-activated solution was added to 0.4 mg of mMPIO in 400 μL citrate buffer pH 5.0. The solution was incubated at 37 ºC and at selected time points 100 μL of solution was taken and 1 μL of the potent cysteine protease inhibitor E-64 (Sigma-Aldrich, UK) solution 1 mM in DMSO was added. After 1 h at 4 ºC the sample was diluted to 700 μL and particle size measured.

In vitro macrophage uptake and degradation experiments

The synthesis of fluorescent labelled mMPIO (with both L- and D- amino acid peptide linkers) and monomeric MPIO was performed as described in **Supplementary Methods 11,12**. RAW264.7 murine macrophage cells (ATCC) were grown in DMEM supplemented with 10% FBS until *ca.* 50% confluent. Cells were incubated with 1 μg of multimeric particles (per 35mm culture dish) for 30 minutes at 37°C. Culture medium was replaced with fresh, pre-warmed complete DMEM, and live cell experiments performed at 37°C using a Zeiss LSM510 laser scanning confocal equipped with a microscope incubator (CO_2 = 5%). Images were collected using a 63X 1.4NA objective, with the 488 nm laser line of an argon laser used for fluorescence and transmitted light imaging. 12 hour time courses were run; imaging interval, 2 minutes. Further experiments were performed in freshly isolated murine macrophages (**Supplementary Method 13**) and the subcellular degradation process was monitored by TEM (**Supplementary Method 14**).

494

495 ***In vivo* mMPIO uptake and clearance experiments**

496

497 Adult male NMRI mice (30 – 40 g) were anaesthetised and injected intravenously with 4 mg
498 Fe/kg body weight of (i) mMPIO-NH_2 or (ii) equivalent sized amine-terminated monomeric
499 MPIO. Animals were transcardially perfused with saline followed by 4% paraformaldehyde
500 at either 1h or 7 days (n = 3 per group) after microparticle injection. Two additional animals
501 were injected with the same dose (4 mg Fe/kg) of mMPIO-COOH and perfused 7 days post-
502 injection. A further group of animals injected with the monomeric MPIO were perfused 14
503 days post-injection (n = 3). All *in vivo* experiments were approved by the UK Home Office.
504 Tissue samples from brain, heart, lung, kidney, liver, spleen and intestine were post-fixed for
505 7 days and paraffin wax embedded. 10 µm sections were dried overnight, de-waxed and
506 stained for iron using Perls´ Prussian Blue stain with a Nuclear Fast Red counterstain. For
507 each tissue, 3 fields of view per animal at 400x magnification were analysed using a semi-
508 automated thresholding method (ImageJ) to determine percentage area of iron staining.
509 Thresholding criteria, based on hue, saturation and luminosity values specific to the
510 microparticles, were constant for each tissue. Differences between groups were assessed
511 using ANOVA followed by post-hoc pairwise t tests with a Welch's correction for unequal
512 variances where appropriate; group sizes were based on previous clearance experiments with
513 commercial MPIO. Mice were assigned randomly to each group, and all analysis was
514 performed blind to the sample groups.
515 Subsequently, a single dose extended acute toxicology study was commissioned from the
516 Commercial Research Organisation Sequani Ltd (full details in **Supplementary Methods**
517 **15,16**). The following assessments were made: body weight, organ weights, macroscopic
518 pathology, haematology and blood chemistry. In addition, microscopic analysis, including
519 assessment of iron deposition, was conducted on brain (at three levels), heart, kidney, liver,

lung and spleen tissue. Subsequent in-house quantitative analysis of Perls´ staining was performed as described above. Group sizes were determined by Sequani Ltd based on previous toxicology work, mice were assigned randomly to each group and analysis was performed blind to sample group.

Synthesis of fluorescently-labelled, targeted mMPIOs

A solution of AlexaFluor 488 SDP ester (2 mg/mL, 250 µL) in DMSO was added to a solution of mMPIO-COOH (5 mL, 1 mg Fe/mL) in sodium bicarbonate buffer 0.1 M pH 8.3. The reaction was shaken for 24 h. Particles were collected using a Dynal magnet (Invitrogen) and washed. Particles were resuspended in 900 µL of MES buffer 0.1 M pH 6.0. SulfoNHS (2 µL, 1 M) in water and EDC (3.5 µL, 0.1 M) in water were sequentially added to 180 µL of the AF488-mMPIO solution. The resultant solution was stirred for 15 minutes at room temperature and then 400 µL of rat anti-mouse VCAM-1 (clone M/K2) or rat IgG_{2a} isotype control antibody (clone KLH/G2a-1-1) (0.5 mg/mL) followed by 400 µL of sodium bicarbonate buffer 0.1 M pH 8.3 was added. The sample was shaken for 24 h. Particles were collected using a magnet (Invitrogen) washed and resuspended in 200 µL of PBS buffer. The antibody loading was determined on multimeric particles from fluorescence intensity using Qifikit calibration beads (Dako, UK) according to the manufacturer's protocol, but substituting the provided fluorescently-conjugated antibody with AlexaFluor594-conjugated rabbit anti-rat IgG (H+L) (Invitrogen, UK; Cat. Nr. A-21211). mMPIO containing 5 µg iron were diluted in 200 µL of 1 x PBS / 0.1% Tween-20. AlexaFluor594-conjugated goat anti-mouse IgG (H+L) (Invitrogen, UK; Cat. Nr. A-11005) (8 µg) was added and incubated at 4°C for 1 hour. The particles were pelleted on a Dynal magnetic separator (Invitrogen) and washed three times with 1 x PBS / 0.1% Tween 20. Flow cytometry experiments were

performed on a BD LSRII flow cytometer and the data analysed using Flow Jo (Tree Star Inc, Oregon, USA).

***In vitro* antibody-mMPIO binding experiments**

Murine endothelial (sEnd.1, PMID: 2736622) cells, cultured in 35 mm dishes cultured in 35 mm dishes (Corning, USA), were stimulated with recombinant mouse TNF-α for 8 hours, fixed with 4 % formaldehyde for 10 minutes at room temperature, washed with PBS and stored at 4 °C. αVCAM-AF488-mMPIO (1.625 μg Fe/mL), IgG-AF488-mMPIO (1.625 μg Fe/mL) or PBS was added to cells and these were placed on a bench-top rocker for 5 minutes at room temperature prior to thorough washing with PBS. Particle binding events were visualized using a 40X, 0.6 NA objective fitted to an Olympus IX-71 microscope.

***In vivo* anti-VCAM-1-targeted experiments**

Adult male NMRI mice (30 – 40 g or 10-12 weeks, n=3) were anesthetized with 2.0-2.5% isoflurane in 70% N_2O: 30% O_2 and stereotaxically microinjected in the left striatum (co-ordinates from Bregma: anterior 0.5 mm, lateral 2 mm, depth 2.5 mm) with 20 ng of recombinant mouse IL-1β in 1 μL low endotoxin saline (n = 3). After 3.1 ± 0.1 h, mice were re-anaesthetised and injected via a tail vein with αVCAM-AF488-mMPIO (4 mg Fe/kg). Three control mice were studied: (i) naïve mouse injected intravenously with αVCAM-AF488-mMPIO as above; (ii) mouse injected intracerebrally with vehicle (1 μL saline) and intravenously with αVCAM-AF488-mMPIO after 3.2 h; and (iii) mouse injected intracerebrally with 20 ng IL-1β in 1 μL saline and intravenously with the non-targeted IgG-AF488-mMPIO after 3.0 h. Following mMPIO injection, animals were positioned in a quadrature birdcage coil. During MRI, anaesthesia was maintained with 1.5-1.8% isoflurane,

568 ECG was monitored and body temperature maintained at ~37°C. All *in vivo* experiments
569 were approved by the UK Home Office.
570
571 **Magnetic resonance imaging**
572 A T_2^*-weighted 3D gradient echo data set was acquired: flip angle = 27°; repetition time (TR)
573 = 65 ms; echo time (TE) = 7.5 ms; field of view (FOV) = 11.2 mm x 22.5 mm x 22.5 mm;
574 matrix size, 96 x 192 x 256; number of averages = 2; total acquisition time ~ 40 min. Mid-
575 point of acquisition was 1.6 ± 0.4 h after microparticle injection. Data were zero-filled to 128
576 x 256 x 256; final isotropic resolution ~ 88 μm. Brains were masked, thresholded and MPIO
577 binding quantified. Spin-echo T_1-weighted images (TR = 500 ms; TE = 20 ms; FOV 25 mm x
578 25 mm; matrix size, 128 x 128) were acquired pre- and 5 min post-Gd-DTPA injection
579 (Omniscan®, GE Healthcare, UK; 30 μl, i.v.). Each T_2^*-weighted data set was converted into
580 tiff images, manually masked to exclude extracerebral structures and converted to 8-bit grey-
581 scale in Adobe Photoshop (Adobe Systems Incorporated, UK). The images were thresholded
582 at a consistent level in the grey channel, such that any pixels of signal intensity > 3 S.D.
583 below the mean intensity of normal brain were set to zero (black) and all others were set to 1
584 (white), see **Supplementary Fig. 39**. The absolute level of thresholding varied between data
585 sets according to variations in signal-to-noise. Signals arising from ventricles or sinuses were
586 excluded by comparison to a naïve animal imaged with no contrast agent, in which these
587 structures appear hypointense naturally. The masked and thresholded images were
588 subsequently imported into ImagePro (Media Cybernetic, UK) and stacked into a single
589 sequence. mMPIO binding, defined as all pixels with signal levels of zero, was quantified in
590 160 consecutive brain slices for each animal. Analysis was performed blind to the origin of
591 the dataset. Segmented images were reconstructed using the 3D Constructor plug-in to
592 visualise the spatial distribution of PIO binding, with low-signal areas assigned to the red

channel and the anatomical image to the green channel. Voxel volumes were summed and expressed as raw volumes in μL with no surface rendering or smoothing effects. Since these were proof-of-principle experiments, to demonstrate the *in vivo* contrast effects of the mMPIO, only a sufficient number of animals was studied to demonstrate that these effects were reproducible and statistical analysis was not performed.

Immunohistochemistry and immunofluorescence

Following MRI, animals were transcardially perfused and the brains post-fixed, cryoprotected, embedded and frozen in isopentane. Expression of VCAM-1 and co-localisation with mMPIO was verified both by immunofluorescence microscopy and immunohistochemically (rat anti-mouse VCAM-1 (clone M/K2)) using avidin-biotin complex amplification.[22] To verify co-localisation of the mMPIO with VCAM-1 expression, Prussian-blue staining to detect iron oxide was performed. Following completion of VCAM-1 immunohistochemistry, some slides were incubated with 20% hydrochloric acid and 10% potassium hexacyanoferrate(II) trihydrate for 20 minutes at 37˚C. After washing with PBS, the slices were then counterstained with cresyl violet.

Microscopy

Images were acquired using either an inverted epifluorescence microscope (DM IRB; Leica Microsystems, Wetzlar, Germany) or an inverted confocal microscope (LSM-710, Carl Zeiss Microimaging, Jena, Germany) and analysed using Image J and Zen (Carl Zeiss) software.

The LSM-710 confocal microscope was equipped with PC-Apochromat 63X 1.2NA oil immersion objective lens. Detection ranges were set to eliminate crosstalk between fluorophores: 409-485 nm for DAPI, 494-553 nm for AlexaFluor 488 and 564-712 nm for Cy3. The set of dichroics MBS 488/561 and MBS-405 were used. The 32 PMT array of the

618 confocal was used to record lambda images which were subsequently unmixed with the Zen
619 software using individually recorded spectra, thus removing inherent autofluorescent signal
620 from the tissue.
621

REFERENCES

1. Gupta, A.K. & Gupta, M. Synthesis and surface engineering of iron oxide nanoparticles for biomedical applications. *Biomaterials* **26**, 3995-4021 (2005).
2. Barry, S.E. Challenges in the development of magnetic particles for therapeutic applications. *Int J Hyperthermia* **24**, 451-466 (2008).
3. Laurent, S., *et al.* Magnetic iron oxide nanoparticles: synthesis, stabilization, vectorization, physicochemical characterizations, and biological applications. *Chem Rev* **108**, 2064-2110 (2008).
4. Weissleder, R., *et al.* Ultrasmall superparamagnetic iron oxide: an intravenous contrast agent for assessing lymph nodes with MR imaging. *Radiology* **175**, 494-498 (1990).
5. Weissleder, R., Bogdanov, A., Neuwelt, E.A. & Papisov, M. Long-circulating iron oxides for MR imaging. *Adv. Drug Deliv. Rev.* **16**, 321-334 (1995).
6. Kievit, F.M. & Zhang, M. Surface Engineering of Iron Oxide Nanoparticles for Targeted Cancer Therapy. *Acc. Chem. Res.* **44**, 853-862 (2011).
7. Lau, J.F., Anderson, S.A., Adler, E. & Frank, J.A. Imaging approaches for the study of cell-based cardiac therapies. *Nat Rev Cardiol* **7**, 97-105 (2010).
8. Haun, J.B., Yoon, T.-J., Lee, H. & Weissleder, R. Magnetic nanoparticle biosensors. *Wiley Interdiscip Rev Nanomed Nanobiotechnol* **2**, 291-304 (2010).
9. Perez, J.M., Josephson, L., O'Loughlin, T., Hogemann, D. & Weissleder, R. Magnetic relaxation switches capable of sensing molecular interactions. *Nat Biotechnol* **20**, 816-820 (2002).
10. Cheon, J. & Lee, J.-H. Synergistically integrated nanoparticles as multimodal probes for nanobiotechnology. *Acc. Chem. Res.* **41**, 1630-1640 (2008).
11. McLachlan, S.J., *et al.* Phase I clinical evaluation of a new iron oxide MR contrast agent. *J Magn Reson Imaging* **4**, 301-307 (1994).
12. Yang, Y., Yang, Y., Yanasak, N., Schumacher, A. & Hu, T.C.C. Temporal and noninvasive monitoring of inflammatory-cell infiltration to myocardial infarction sites using micrometer-sized iron oxide particles. *Magn Reson Med* **63**, 33-40 (2010).
13. Weissleder, R., Kelly, K., Sun, E.Y., Shtatland, T. & Josephson, L. Cell-specific targeting of nanoparticles by multivalent attachment of small molecules. *Nat Biotechnol* **23**, 1418-1423 (2005).
14. Tassa, C., *et al.* Binding Affinity and Kinetic Analysis of Targeted Small Molecule-Modified Nanoparticles. *Bioconjugate Chem.* **21**, 14-19 (2009).
15. Akhtar, A.M., *et al.* In vivo quantification of VCAM-1 expression in renal ischemia reperfusion injury using non-invasive magnetic resonance molecular imaging. *PLoS One* **5**, e12800 (2010).
16. McAteer, M.A., *et al.* In vivo magnetic resonance imaging of acute brain inflammation using microparticles of iron oxide. *Nat Med* **13**, 1253-1258 (2007).
17. van Kasteren, S.I., *et al.* Glyconanoparticles allow pre-symptomatic in vivo imaging of brain disease. *Proc. Natl. Acad. Sci., USA* **106**, 18-23 (2009).
18. von zur Muhlen, C., *et al.* Magnetic resonance imaging contrast agent targeted toward activated platelets allows in vivo detection of thrombosis and monitoring of thrombolysis. *Circulation* **118**, 258-267 (2008).
19. McAteer, M.A., *et al.* Magnetic resonance imaging of endothelial adhesion molecules in mouse atherosclerosis using dual-targeted microparticles of iron oxide. *Arterioscler Thromb Vasc Biol* **28**, 77-83 (2008).
20. Hoyte, L.C., *et al.* Molecular magnetic resonance imaging of acute vascular cell adhesion molecule-1 expression in a mouse model of cerebral ischemia. *J Cereb Blood Flow Metab* **30**, 1178-1187 (2010).
21. von zur Muhlen, C., *et al.* A contrast agent recognizing activated platelets reveals murine cerebral malaria pathology undetectable by conventional MRI. *J Clin Invest* **118**, 1198-1207 (2008).
22. Serres, S., *et al.* Molecular MRI enables early and sensitive detection of brain metastases. *Proc. Natl. Acad. Sci., USA* **109**, 6674–6679, (2012).
23. Kanke, M., Simmons, G.H., Weiss, D.L., Bivins, B.A. & Deluca, P.P. Clearance of 141Ce-labeled microspheres from blood and distribution in specific organs following intravenous and intraarterial administration in beagle dogs. *Journal of Pharmaceutical Sciences* **69**, 755-762 (1980).
24. Illum, L., *et al.* Blood clearance and organ deposition of intravenously administered colloidal particles. The effects of particle size, nature and shape. *International Journal of Pharmaceutics* **12**, 135-146 (1982).
25. Normann, S. Kinetics of Vascular Clearance of Particles by Phagocytes. in *Physiology* (eds. Reichard, S.M. & Filkins, J.P.) 73-101 (Springer US, 1984).
26. Sun, E.Y., Josephson, L., Kelly, K.A. & Weissleder, R. Development of nanoparticle libraries for biosensing. *Bioconjugate Chem.* **17**, 109-113 (2006).

27. Doronina, S.O., *et al.* Development of potent monoclonal antibody auristatin conjugates for cancer therapy. *Nat Biotech* **21**, 778-784 (2003).
28. Leriche, G., Chisholm, L. & Wagner, A. Cleavable linkers in chemical biology. *Bioorganic & Medicinal Chemistry* **20**, 571-582 (2012).
29. Mohamed, M.M. & Sloane, B.F. Cysteine cathepsins: multifunctional enzymes in cancer. *Nat Rev Cancer* **6**, 764-775 (2006).
30. Weissleder, R., *et al.* Superparamagnetic iron oxide: pharmacokinetics and toxicity. *AJR Am J Roentgenol* **152**, 167-173 (1989).
31. Chouly, C., Pouliquen, D., Lucet, I., Jeune, J.J. & Jallet, P. Development of superparamagnetic nanoparticles for MRI: effect of particle size, charge and surface nature on biodistribution. *J Microencapsul* **13**, 245-255 (1996).
32. Schulze, E., *et al.* Cellular uptake and trafficking of a prototypical magnetic iron oxide label in vitro. *Invest. Radiol.* **30**, 604-610 (1995).
33. Rawlings, N.D., Barrett, A.J. & Bateman, A. MEROPS: the peptidase database. *Nucleic Acids Res* **38**, D227-233 (2010).
34. Cotrin, S.S., *et al.* Positional-scanning combinatorial libraries of fluorescence resonance energy transfer peptides to define substrate specificity of carboxydipeptidases: assays with human cathepsin B. *Anal Biochem* **335**, 244-252 (2004).
35. Choe, Y., *et al.* Substrate profiling of cysteine proteases using a combinatorial peptide library identifies functionally unique specificities. *J Biol Chem* **281**, 12824-12832 (2006).
36. Staros, J.V. N-hydroxysulfosuccinimide active esters: bis(N-hydroxysulfosuccinimide) esters of two dicarboxylic acids are hydrophilic, membrane-impermeant, protein cross-linkers. *Biochemistry* **21**, 3950-3955 (1982).
37. Terada, M. A novel role in the removal of blood-borne foreign bodies for pulmonary capillaries in the guinea pig. *Virchows Arch B Cell Pathol Incl Mol Pathol* **63**, 147-157 (1993).
38. Pittet, M.J., Swirski, F.K., Reynolds, F., Josephson, L. & Weissleder, R. Labeling of immune cells for in vivo imaging using magnetofluorescent nanoparticles. *Nat. Protocols* **1**, 73-79 (2006).

FIGURE LEGENDS

Figure 1. Molecular basis of mMPIO as a targeted MRI contrast agent. Intravenously injected targeted mMPIO bind to their target on the diseased endothelial surface (i), but do not bind to healthy endothelium (ii). The unbound mMPIO are rapidly cleared from blood. Thus, negligible background contrast effects are evident with mMPIO shortly after injection. mMPIO are efficiently taken up by macrophages (iii), and after internalisation and fusion to lysosomes the internal peptide linkers are degraded. mMPIO are represented as brown sphere conglomerates, iron oxide nanoparticles are represented as blue and brown spheres, targeting agents are represented in dark blue and endothelial surface disease markers are shown in green.

Figure 2. Schematic representation of the synthesis of mMPIO. Grey spheres represent amine-functionalized dextran coated iron oxide nanoparticles, blue spheres represent peptido-

NPs and brown spheres represent carboxy-NPs. Conditions: (i) peptide **3**, *N*-(3-dimethylaminopropyl)-*N*′-ethylcarbodiimide hydrochloride (EDC) *N*-hydroxysuccinimide (NHS), 2-(N-morpholino)ethanesulfonic acid (MES) buffer (0.1 M pH6.0)/ dimethylsulfoxide (DMSO) 1:1; (ii) piperidine/ *N*,*N*-dimethylformamide (DMF)/DMSO (2:3:5); (iii) succinic anhydride, sodium bicarbonate buffer (0.1M pH 8.3)/DMSO 1:1; (iv) EDC, sulfoNHS, MES buffer (0.1M pH 6.0); (v) when an excess of carboxy-NPs are used a mMPIO with excess surface carboxylic acid functions is formed; when an excess of peptido-NPs is employed the mMPIO surface contains excess amine functions (not shown).

Figure 3. Physicochemical characterization of mMPIO. (a) Size and yield of mMPIO as a function of carboxy-NP/peptido-NP ratio. [a] ratio between carboxy-NPs and peptido-NPs (w/w); [b] determined by dynamic light scattering (DLS). **(b)** Microscopic characterization of mMPIOs by TEM (top three images showing different representative examples; scalebars left-to-right 100, 100 and 50 nm), AFM (bottom left, scalebar 50 nm) and HRTEM (bottom middle and right; bottom right is the inset magnification from bottom middle; scalebars 50 and 5 nm). **(c)** DLS size distribution graph of ~700 nm mMPIO just after synthesis (red line) and after storage for 6 months (blue line). **(d)** T_2 weighted images of the phantoms (iron concentration = 0.224 mM) at echo times 9.7 ms (left) and 16.3 ms (right).

Figure 4. *In vitro* and *in vivo* degradation studies. (a) DLS analysis of particle size distribution of mMPIO after addition of cathepsin L. Particle size was analyzed at different time points 0 h (red line), 1 h (blue line), 4 h (light green), 8 h (purple) and 24 h (dark green). Experiments were performed in triplicate. **(b)** Time-course montage of particle degradation by the murine macrophage cell line RAW264.7 obtained by live cell confocal imaging. Visible particles are indicated by black arrows. Experiments were performed in triplicate.

747 Scalebar 10μm. **(c)** Graph to show distribution of *ca*. 700 nm mMPIO and MPIO in different
748 organs 1 h and 7 days after intravenous injection (n=3 per group). Data are mean ± SD for 3
749 fields per organ. *P<0.05 based on one-way ANOVA on a tissue-wise basis followed by
750 Newman-Keuls post-hoc tests. **(d)** Images of immunohistochemical sections taken from
751 different organs 1 h and 7 days after intravenous injection of either mMPIO or MPIO.
752 Sections have been stained with Prussian Blue to identify iron and counterstained with
753 Nuclear Fast Red. Magnification is 400X, scale bar = 50 μm.
754
755 **Figure 5.** ***In vivo*** **VCAM-1-targeting experiments. (a-b)** Selected T_2*-weighted images
756 from 3D datasets obtained from mice injected intrastriatally with IL-1β 3 hours before
757 intravenous injection of either **(a)** αVCAM-AF488-mMPIO or **(b)** control non-targeted IgG-
758 AF488-mMPIO. Focal hypointense areas (black) in the left hemisphere reflect the specific
759 αVCAM-AF488-mMPIO retention on acutely activated vascular endothelium **(a)**, with
760 negligible contrast effects evident in either the contralateral control hemisphere or in the
761 animal injected with IgG-AF488-mMPIO **(b)**. Box indicates the injected hemisphere. **(c-d)**
762 3D reconstructions of the mMPIO-induced hypointensities (coloured in red) from mice
763 injected with either αVCAM-AF488-mMPIO **(c)** or IgG-AF488-mMPIO **(d)** shown both as a
764 stacked plot (left) and within the mouse brain frame of reference (right). Negligible contrast
765 effects are evident in the animal injected with IgG-AF488-mMPIO. **(e)** Graph to show
766 volumes of hypointensities in αVCAM-AF488-mMPIO injected mice (black circles; n=3)
767 and controls (black square IL-1β + IgG-AF488-mMPIO; black triangle, saline + IgG-AF488-
768 mMPIO; black diamond, naïve + αVCAM-AF488-mMPIO). Data are shown as specific
769 contrast (left-right difference) for each animal; note negligible specific contrast is apparent in
770 the control mice. Each data point represents an individual mouse; since this was a proof-of-
771 principle experiment to demonstrate in vivo contrast effects, statistical analysis was not

performed. **(f-i)** Immunohistochemical and immunofluoresence images of brain sections taken from IL-1β-injected mice. **f (i, ii)** Immunohistochemical sections showing VCAM-1 expression (brown) co-localised with αVCAM-AF488-mMPIO (Prussian Blue staining). Epifluorescence (**g (i)**) and confocal (**g (ii)**) images further demonstrate adherence of αVCAM-AF488-mMPIO (green) to VCAM-1-positive (red) vessels. Nuclei are stained with DAPI (blue). Additional alkaline phosphatase staining enabled co-localisation of αVCAM-AF488-mMPIO (green) with VCAM-1 (blue) and vessels (laminin – red) to be confirmed using both epifluorescence (**h (i)**) and confocal (**h (ii)** and **i (i, ii))** microscopy. Arrows indicate αVCAM-AF488-mMPIO. Scale bars = 10 μm (f (i,ii); h (ii); i (i,ii)) and 5 μm (g (i,ii); h (i)).

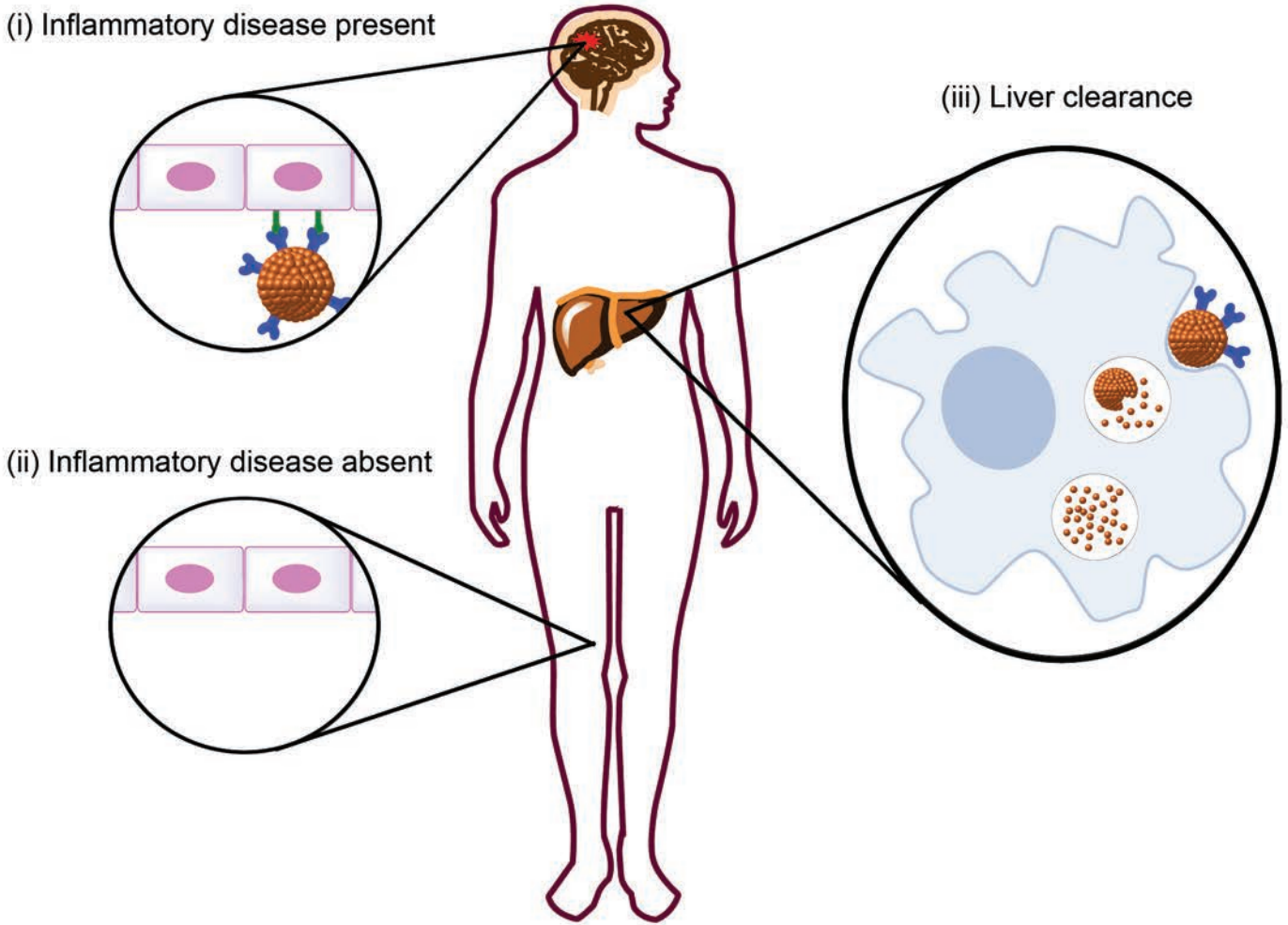
(i) Inflammatory disease present
(iii) Liver clearance
(ii) Inflammatory disease absent

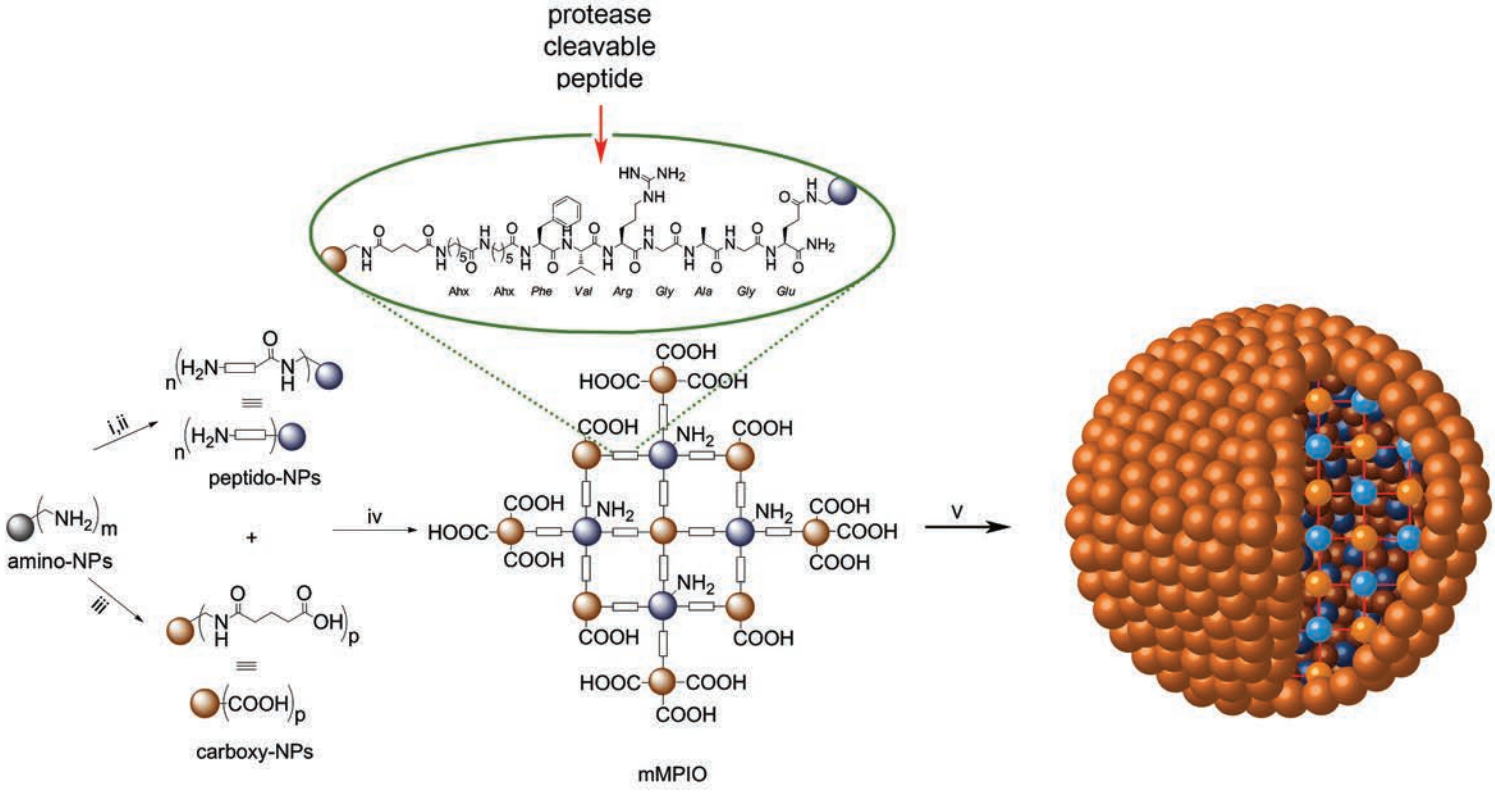
protease
cleavable
peptide
Ahx Ahx Phe Val Arg Gly Ala Gly Glu
i,ii
peptido-NPs
amino-NPs
+
iii
carboxy-NPs
iv
mMPIO
v

a

	Particle ratio[a]	Size (nm)[b]
1	1:8	250
2	1:7	450
3	1:6	711
4	1:5	1569
5	1:4.5	2279
6	6:1	504
7	5.5:1	808

b

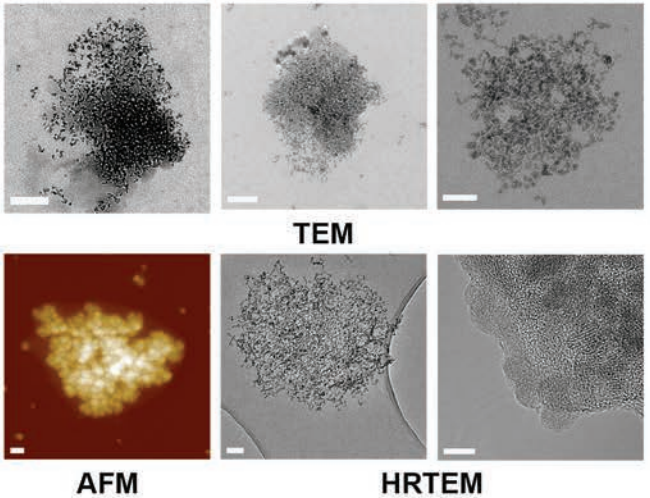

c

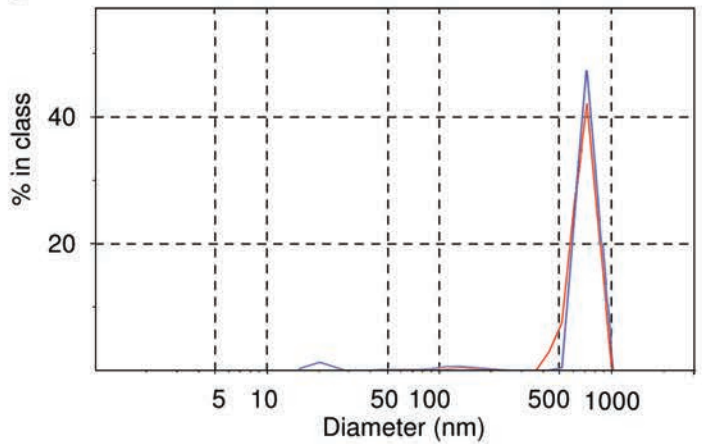

d

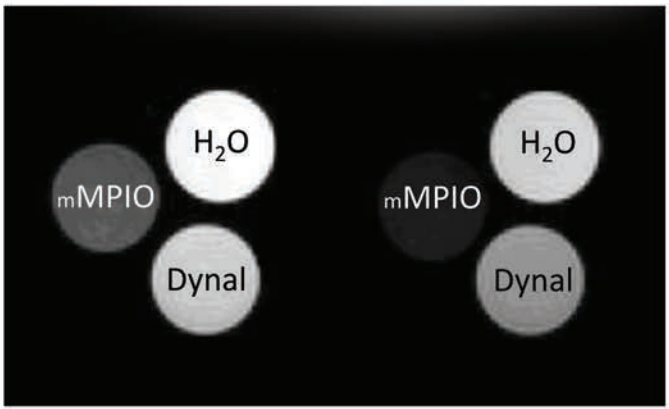

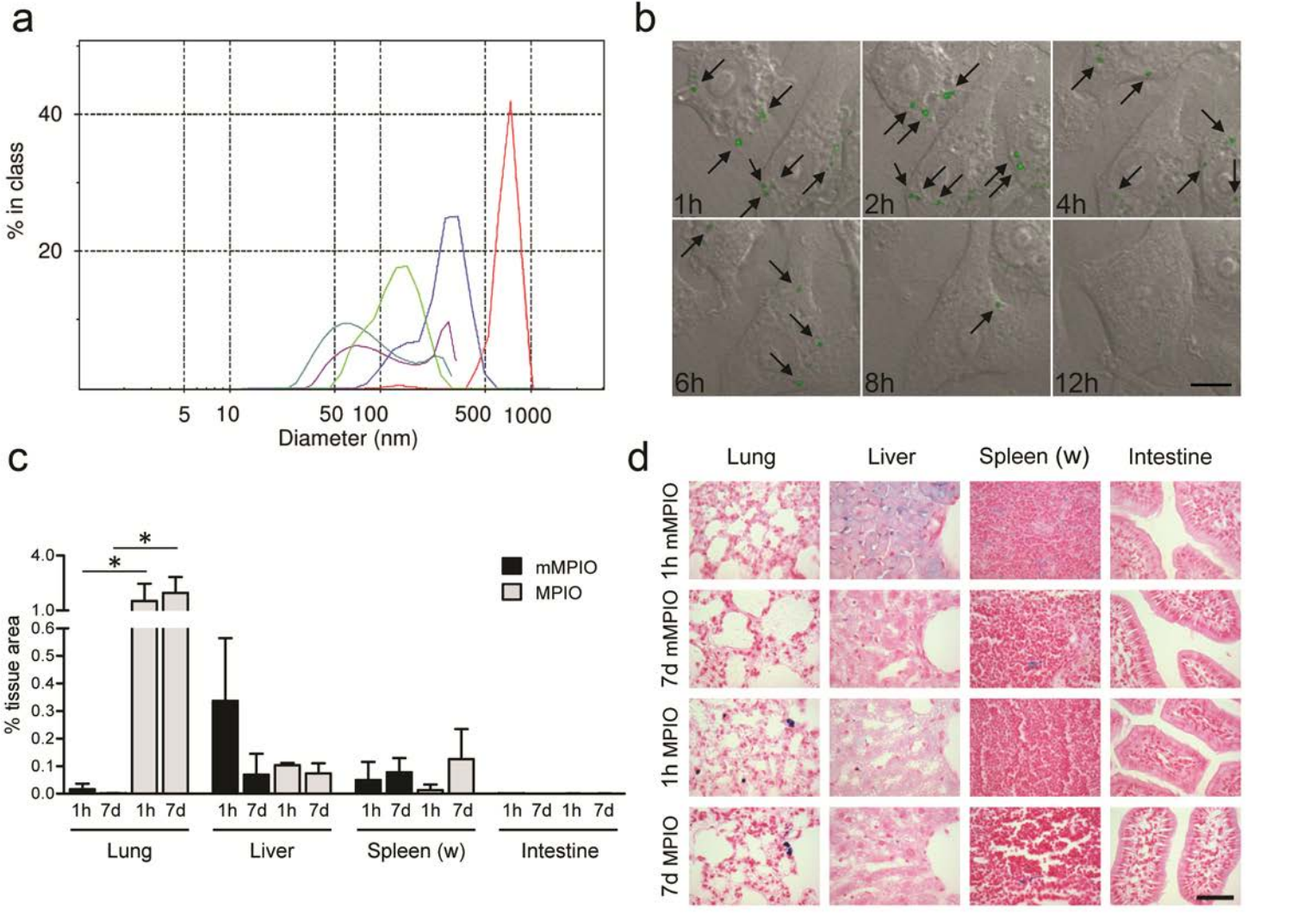
a
% in class
40
20
5
10
50
100
500
1000
Diameter (nm)
b
1h
2h
4h
6h
8h
12h
c
% tissue area
4.0
1.0
0.6
0.5
0.4
0.3
0.2
0.1
0.0
*
*
mMPIO
MPIO
1h 7d 1h 7d
Lung
1h 7d 1h 7d
Liver
1h 7d 1h 7d
Spleen (w)
1h 7d 1h 7d
Intestine
d
Lung
Liver
Spleen (w)
Intestine
1h mMPIO
7d mMPIO
1h MPIO
7d MPIO

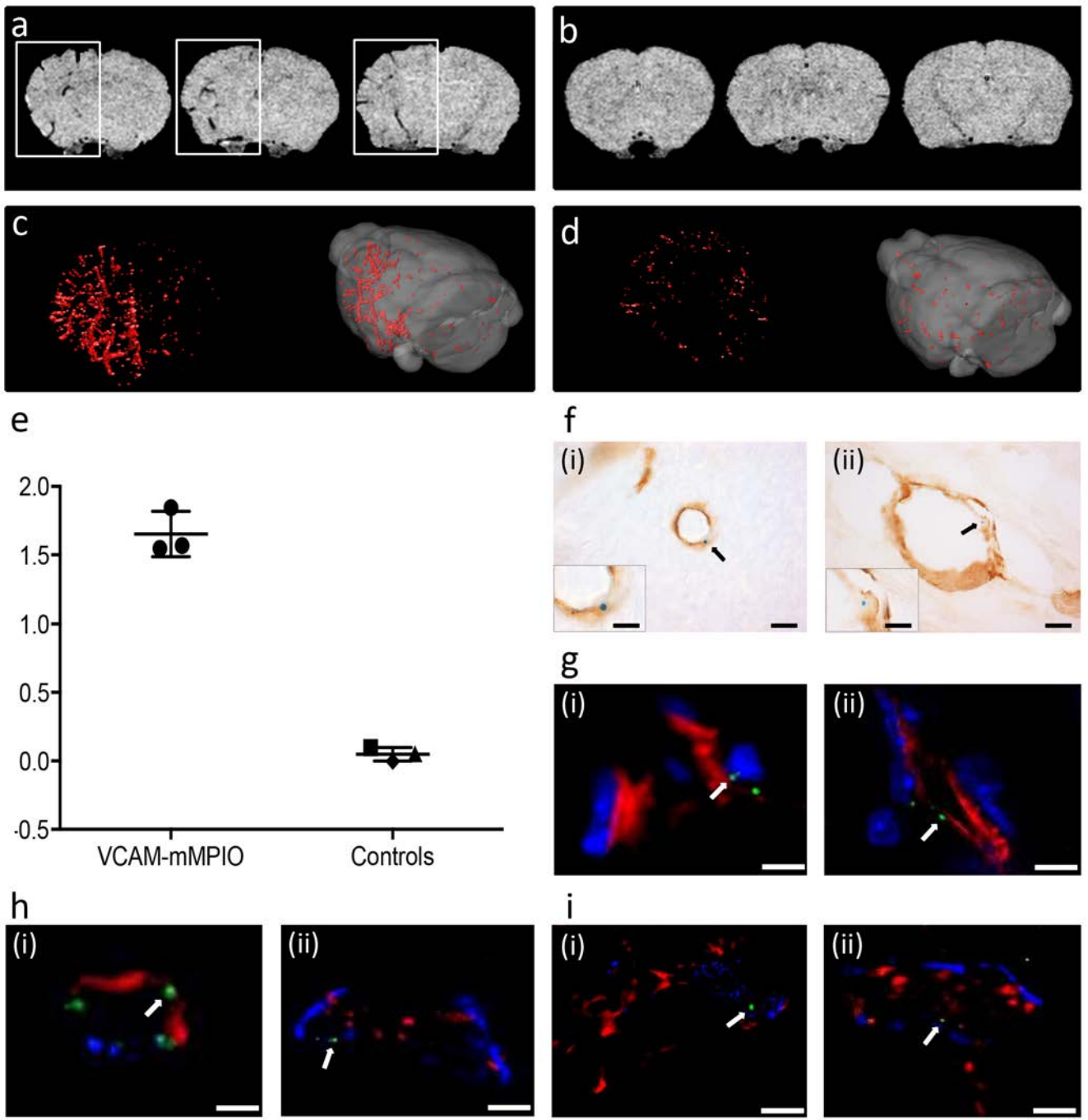
a
b
c
d
e
2.0
1.5
1.0
0.5
0.0
-0.5
VCAM-mMPIO
Controls
f
(i)
(ii)
g
(i)
(ii)
h
(i)
(ii)
i
(i)
(ii)